

# Using Bayesian Neural Network to Solve the Inverse Problem in Electrical Impedance Tomography

Jouko Lampinen and Aki Vehtari  
Laboratory of Computational Engineering  
Helsinki University of Technology  
P.O.Box 9400, FIN-02015  
Espoo, FINLAND

Kimmo Leinonen  
Ahlstrom Pumps Corporation  
P.O.Box 18, FIN-48601  
Karhula, FINLAND

## Abstract

In this contribution we present a method for solving the inverse problem in electric impedance tomography with Bayesian MLP neural network. The problem of reconstructing the conductivity distribution inside an object from potential measurements from the surface is known to be ill-posed, requiring efficient regularization techniques. We decompose the reconstruction problem to lower dimensional problem by principal component projection, and use very efficient Bayesian neural network to solve the reduced problem. This approach contains double regularization effect, first due to solving the inverse problem in the eigenspace, and second due to using neural networks that learn the distribution of feasible solutions from the training data. We show by simulations, that the proposed approach leads to rather accurate reconstruction results and facilitates estimation of other target values, such as the void fraction (the fraction of gas in liquid), directly without actual image reconstruction. We also demonstrate that the solutions are very robust against noise in inputs.

## 1 Introduction

In electrical impedance tomography, EIT, the aim is to recover the internal structure of an object from surface measurements. Number of electrodes are attached to the surface of the object and current patterns are injected from through the electrodes and the resulting potentials are measured. The inverse problem in EIT, estimating the conductivity distribution from the surface potentials, is known to be severely ill-posed, so that some regularization methods must be used to obtain feasible results [1].

Fig. 1 shows an simulated example of the EIT prob-

lem. The volume bounded by the circles in the image represent gas bubble floating in liquid. The conductance of the gas is much lower than that of the liquid, producing the equipotential curves shown in the figure. Fig. 2 shows the resulting potential signals, from which the image is to be recovered.

Typically, the inverse problem in EIT is solved by assuming the system linear and computing regularized inverse matrix. This produces fast linear reconstruction algorithm. However the linear assumption is valid only if the perturbation from the linearization point is small, i.e., there are no large areas where conductance differs much from the background.

Another, more accurate approach for the image reconstruction in EIT is based on iterative inversion of the forward problem. Numerical minimization method, such as Newton-Raphson algorithm, is used to search for a conductance distribution that minimizes the difference between the measured potentials and those obtained by computing the potentials by, e.g., finite element method. This approach leads to computationally more complex algorithms, but gives much better results and offers more flexibility for controlling the regularization of the inverse, by defining the smoothing priors for the resulting image [1].

In this contribution we propose a feedforward solution for the reconstruction problem that can take into account the nonlinearities in the forward (and inverse) problems. The approach is based on approximating the inverse mapping from the eigenspace of the potential signals to the eigenspace of the conductivity distributions with a Bayesian neural network. Often the end goal of using process tomography is not the reconstructed image, but some index computed from the image, such as void fraction (proportion of gas in liquid) or mixing index indicating how well two substances have been

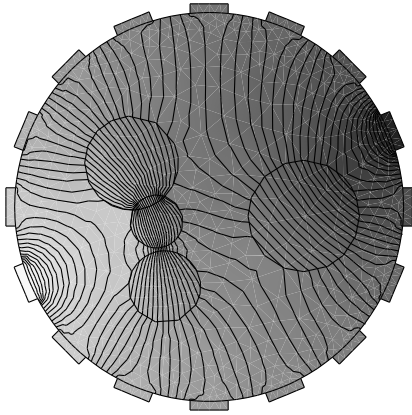


Figure 1: Example of the EIT measurement. The simulated bubble formation is bounded by the circles. The current is injected from the electrode with the lightest color and the opposite electrode is grounded. The gray level and the contour curves show the resulting potential field.

mixed. We demonstrate that in such situation it may be feasible to directly estimate the target variable without the actual image reconstruction. Estimating the void fraction, for example, is shown to be much lower dimensional problem than recovering the distribution of the gas.

There are a few studies on using neural networks in the EIT problem. In [2] the reconstruction image was directly estimated by a NN from the potential signals. The solution was demonstrated to be very robust against noise in input signals. However, the resolution of the image in such approach is in practice limited to some tens or hundreds of pixels, as networks with several hundreds of outputs are rather difficult to use and train, and often require non-standard regularization to smooth the results of neighboring pixels.

In [3] linear neural network was used to estimate the conductance in the triangles of the FEM mesh. As the used network was linear, the actual advantage over linear pseudoinverse solutions was due to the iterative estimation of the inverse matrix with a gradient method, which proceeds slowly to the direction of the smallest eigenvectors of the inverse matrix, yielding natural regularization for the inverse.

In [4] combination of principal component analysis (PCA) and neural network was used for computing a scalar variable, mixing index, from reconstructed tomographic images. Our results indicate that direct estimation of the target variables without the explicit reconstruction may be appropriate solution, as the reconstruction may be much more complex problem than the actual end goal.

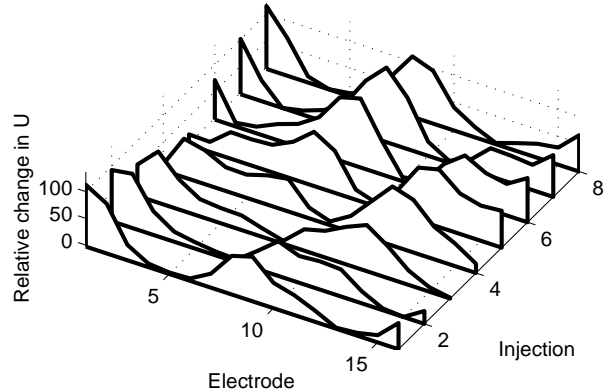


Figure 2: Relative changes in potentials compared to homogeneous background. The eight curves correspond to injections from eight different electrodes.

## 2 Simulated EIT Problem

In this study we have considered a simulated EIT problem. The aim is to recover the shape of a gas bubble in liquid flowing in a circular pipe. The conductivity of the gas was much lower (1/100) than that of the liquid and the size of the bubble was large (upto 50% of the area) so that linear reconstruction was not applicable. In addition to the reconstruction of the bubble shape, an important goal in the process tomography application we are studying is to estimate the void fraction, which is the relative area of the gas bubble compared to the area of the pipe.

We produced the data by defining a Gamma-distribution for the void fraction with mean at about 20 % and range in about 5 % to 50 %. Then we draw void fraction values and overlaid random circular bubbles with radius  $r \sim Uniform(0.05, 0.35)$  on the image, until the drawn void fraction was complete. The bubble formations contained 1 to 10 circles with average of 4 circles in each image. The simulation of the forward problem was computed with FEM (Finite Element Method) using Matlab PDE-toolbox.

The training data for the neural network contained 500 samples of the bubbles and the test data another 500 samples. All the results reported are computed from the test data that has not been used in any way during the building of the model.

## 3 Eigenimage decomposition

In the proposed approach we apply the neural network in a low dimensional eigenspace, where linear depen-



Figure 3: Eigenimages of the simulation data

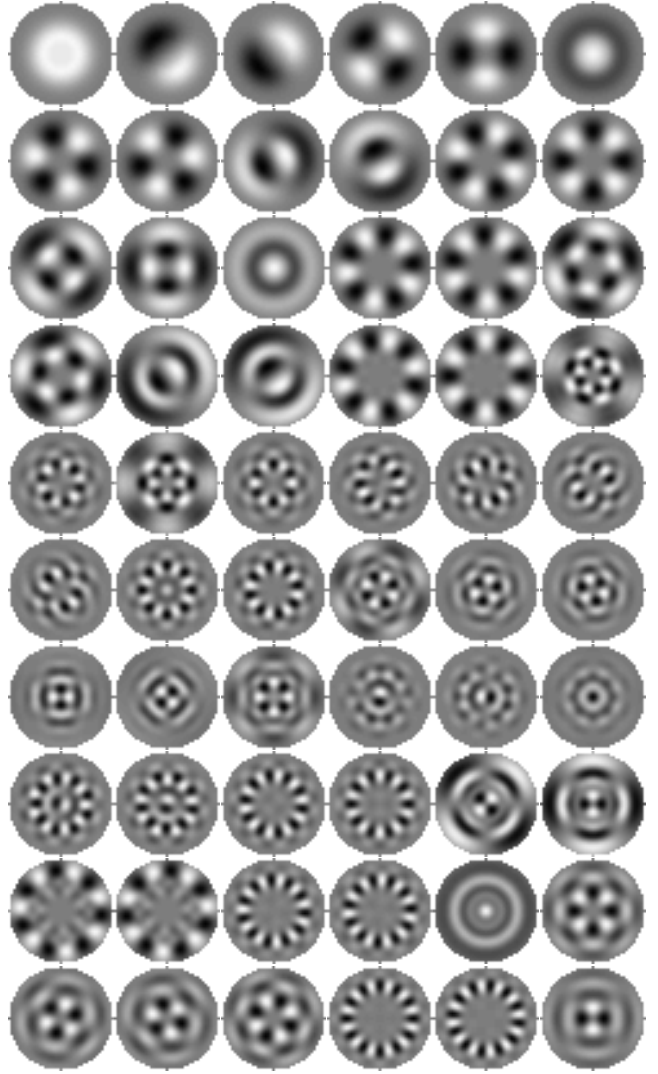


Figure 4: Eigenimages from the autocorrelation model in Eqs. 2 and 3.

dencies from the input and output variables have been removed. This serves for three purposes: first to detach the actual inverse problem from the data representation of the potential signals and image data, allowing change of image resolution afterwards by changing the resolution of the eigen images. Secondly, the reconstruction of the image as superposition of the eigen images of true bubble shapes makes the inverse robust against noise, as shown by the experiments. Thirdly, the dimensionality of the reconstruction problem is much reduced, and it is matched to the actual complexity of the bubble distributions (determined by the eigenvalues of the correlation matrix). Direct reconstruction of each pixel separately would be more prone to get overfitted to the training data, and would require additional non-standard regularization to smooth the result between neighboring pixels, just as in iterative inverse methods.

The reconstruction equations are then

$$\begin{aligned} u_p &= V_u u \\ g_p &= F(p) \\ g &= V_g^T g_p \end{aligned} \tag{1}$$

where

- $u$  is the potential signal,
- $V_u$  is the base span by the largest eigenvectors of  $u$  (we used  $N_u = 20$ ),
- $u_p$  is the projection of  $u$  on  $V_u$ ,
- $g$  is the reconstructed image,
- $V_g$  is the base of eigenvectors of the autocorrelation matrix of the images,
- $g_p$  is the projection of the image  $g$  on base  $V_g$ , and
- $F(p)$  is the non-linear function giving the inverse (the Bayesian MLP).

The base images given by the PCA depend only on the autocorrelation of the images, as the base consists of the eigenvectors of the autocorrelation matrix. Thus we can construct the base directly by making assumption for the autocorrelation of the bubbles. Then the base images are not computed from the training data, making the base more general and less tuned to the particular set of training images.

The autocorrelation model for the bubbles consisted of position dependent variance term  $S(x, y)$  and position independent autocorrelation term  $A(\Delta x, \Delta y)$ :

$$R_{xy, x'y'} = A(x - x', y - y')S(x, y)S(x', y'), \quad (2)$$

where we used rather generic assumptions: autocorrelation of pixels decays linearly as function of distance  $\sqrt{\Delta x^2 + \Delta y^2}$  and reaches zero correlation at distance 0.5 (half of the radius of the pipe). The variance was modeled as sum of two Gaussians

$$S(x, y) = \sum_{k=1}^2 Z_k \exp\left(-\frac{x^2 + y^2}{2\sigma_k^2}\right). \quad (3)$$

where the parameters  $\sigma_k$  and  $Z_k$  were determined by maximum likelihood fit to the training data. The values were  $Z_1 = 1.07$ ,  $Z_2 = -0.58$ ,  $\sigma_1 = 0.31$ ,  $\sigma_2 = 0.06$ . Note that we can control the accuracy of image representation by this base in different location of the image by changing the autocorrelation length. Smaller autocorrelation results in more eigenimages coding the location and vice versa.

Figs. 3 and 4 show the eigenvectors of the simulated bubbles and those from the autocorrelation model. The resolution of the images is  $41 \times 41$  pixels, which is probably more than needed in most applications.

Most of the eigenimages in Fig. 4 code only the shape of the bubble and have zero mean. Consequently, only very few eigenimages contribute to the void fraction. This can be seen from Fig. 5, which shows the relative error in the void fraction, when the bubble image is projected to the subspace of the eigenimages and then reconstructed from the projection. The flat areas correspond to zero mean eigenvectors. Note that the error shown in Fig. 5 is the residual error that would be left even if the inverse were exact in the eigenspace.

## 4 Bayesian Neural Networks

Traditionally neural networks have been trained by searching for a set of weights that minimize the error between the target values and network outputs.

In Bayesian learning the objective is to find the predictive distribution for output  $y$  given the input  $x$  and training data  $D$  (see [5] and [6] for introduction to

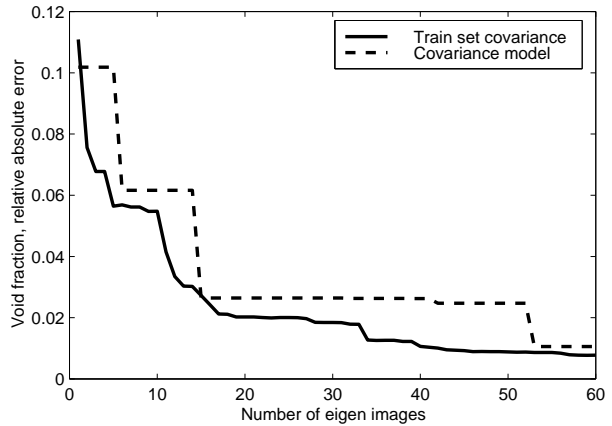


Figure 5: Relative error in void fraction due to the PCA projection as function of the base dimension.

Bayesian neural networks)

$$p(y|x, D) = \int p(y|x, w, \beta) \frac{p(D|w)p(w|\alpha)p(\alpha)}{p(D)} dw, \alpha, \beta \quad (4)$$

where we compute the marginal distribution over all the parameters  $w$  and hyperparameters  $\alpha$ , that determine the prior distributions for parameters, and  $\beta$ , that define the noise variance. Intuitively, the marginalization is equal to taking the average prediction of all the models  $p(y|x, w, \beta)$  weighted by their goodness, which is the posterior probability of the model given the training data  $D$ . In practice we use Markov Chain Monte Carlo techniques for approximating the integral by mean of samples drawn from the posterior distribution of the models [6]. In the following experiments we have used the FBM software package<sup>1</sup> that implements the methods described in [6]. The resulting model after the learning is a collection of networks with different parameters  $w$ , such that the average of the outputs of the networks approximates the conditional expectation of the output given the input. In this work we have used 20 samples from the posterior distributions (sampled sparsely from the end of long MCMC runs), so that the network model is equal to having a committee of 20 networks.

### Advantages of Bayesian MLP networks

- Bayesian learning provides automatic complexity control: by integrating over the hyperparameters that determine the model complexity, all the models with different effective complexity are weighted in the result by their posterior probability given the data.

<sup>1</sup><URL: <http://www.cs.toronto.edu/~radford/fbm.software.html>>

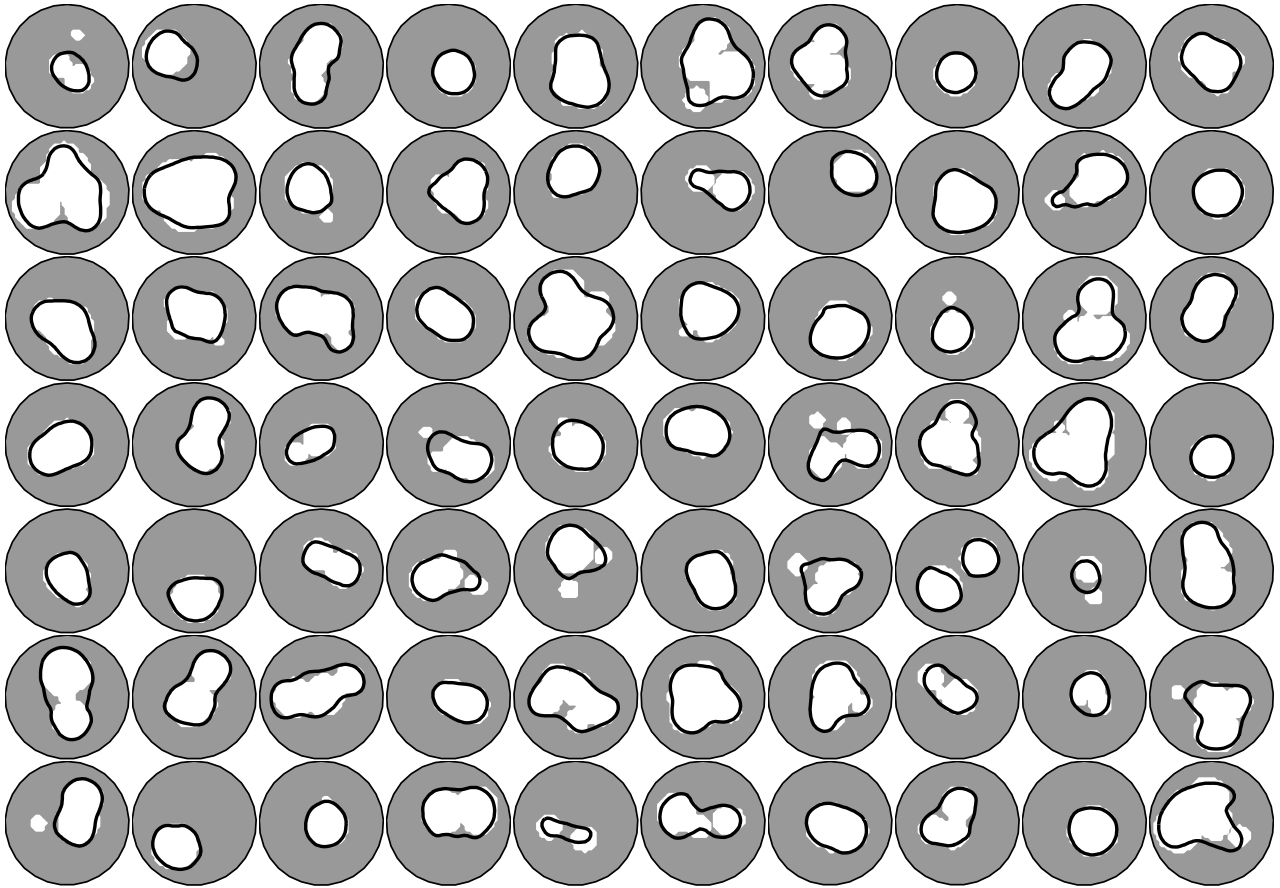


Figure 6: Examples of reconstructed bubble formations. The white blobs show the actual simulated bubbles and the black lines show the contours of the reconstructed bubbles. All the bubbles are from the test set that has not been used in the training in any way.

- We can use large networks with small risk of overfitting, and there is no need to find the minimum sufficient number of weights in the model.
- The model gives the predictive distribution for the outputs, providing confidence interval for the estimates.
- Possibility to use various types of prior information and hierarchical models for hyperparameters.

## 5 Simulation Results

### 5.1 Image Reconstruction

In this contribution we report only results on using Bayesian MLP model for the inverse problem. For comparison with other training methods see [7].

The goodness of the reconstructed images was evaluated both visually and using a quantitative error criterion. The error was defined as the percentage of pixels in the image whose classification to gas bubble/liquid

was erroneous.

In the following experiments we used  $N_g = 30$  eigenimages to reconstruct the image. Fig. 6 shows some sample reconstructions from the test set. The actual output of the network committee is the conditional mean of the image given the potential signals, which is equal to the conditional probability of a pixel being in a bubble with the used coding of bubble as 1 and background as 0. Then the void fraction, i.e., the total amount of gas, is obtained by computing the total probability mass of bubbles over the image. The images were segmented to gas and background as follows (see Fig. 8 for examples):

1. The void fraction is estimated as the sum of bubble probability over the image.
2. Segmentation threshold is selected so that the void fraction is preserved (i.e., the size of the segmented bubble is equal to the void fraction.)
3. The pixels are segmented to either gas or background class, as shown in Figs. 6 and 8.

The mean error in the test set was 3.96 %.

## 5.2 Estimation of the Void Fraction

The most important end variable in the studied application was the void fraction. As shown in previous chapter, in the eigenspace of the bubble images the problem of reconstructing the void fraction has only very low complexity compared to that of recovering the shape of the gas distribution. Thus it is reasonable to estimate the void fraction directly without first reconstructing the image.

Fig. 7 shows the scatter plot of estimating the void fraction directly and reconstructing the image first and computing the void fraction from the image. The goodness of the estimate was measured by the mean relative absolute error,  $E = 1/N \sum_n |v_n - \hat{v}_n|/v_n$ , where  $v_n$  is the actual void fraction and  $\hat{v}_n$  the estimate for bubble sample  $n$ . The errors were 3.15 % and 5.96 % for direct estimation of the void fraction and estimation of the void fraction from the reconstructed image, respectively.

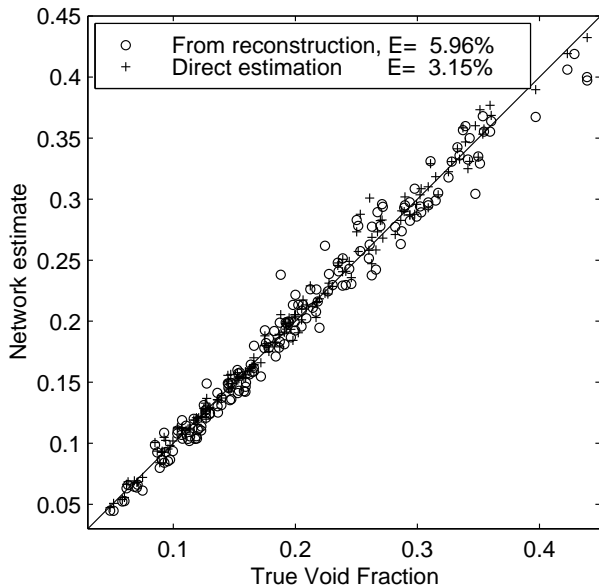


Figure 7: Scatter plot of the void fraction estimates from the reconstructed image and directly from the potential signals.

## 5.3 Robustness to Noise

A special virtue of the solution proposed here is very high robustness to noise. Similar property of the NN inverse was also reported in [2]. In the current approach the PCA projection of the potential signal and images contributes to the suppression of noise effects, as uncorrelated noise is also largely uncorrelated with the eigenvectors of the signals. The NN solution to the inverse, so called direct inverse, is based on estimating the conditional expectation of the image given the potentials.

The network approximates the inverse mapping with a continuous function, whose smoothness is determined from the training data by the Bayesian estimation procedure. When the inverse is not stable, so that small changes in the potentials cause large changes in the images, the training data for the network contains different output images for nearly equal inputs, which is statistically the same as having noise in the outputs. Thus the instability of the inverse causes the estimate of the noise variance to increase and consequently the posterior distribution to become broader. This causes the approximation to become smoother when more varying models are summed in Eq. 4.

Fig. 9 shows the effect of noise on the inputs to the direct estimation of the void fraction. The noise was additive Gaussian noise with standard deviation given as percentage of the maximum amplitude of the potential signal. Fig. 10 shows the effect of noise to the image reconstruction results. The error is computed as percentage of pixels that are erroneously segmented to belong to the bubble or background by the network. Note that the expected noise level in industrial environment is about 2-5 %, which should have no significant effect to the inverse solutions by the proposed techniques. Fig. 8 shows examples of the reconstructed images from the noisy potential measurements.

## 6 Conclusion

In this contribution we have demonstrated that Bayesian neural network can be used for solving the ill-posed inverse problem in electrical impedance tomography. With Bayesian neural network we can use large number of free parameters in the model with no fear of overfitting (given that our prior distributions and noise models are feasible). With the proposed system the inverse can be computed in a feedforward manner, facilitating real-time monitoring of the process. Also the solution is demonstrated to be highly immune to noise.

Often one of the end goals in the process tomography is to compute some performance index variables from the reconstructed image. We demonstrate that it may be feasible to recover such variables directly from the measurements without solving the actual tomographic reconstruction problem. For example, estimating the void fraction (proportion of gas in liquid) is shown to be a lower dimensional subproblem of the image reconstruction. Consequently, the void fraction can be estimated to higher accuracy directly from the measurements.

Currently we are running experiments to compare this approach to state-of-the-art iterative methods. Also we will test the method with real data in cooperation with the industrial partner of the project.

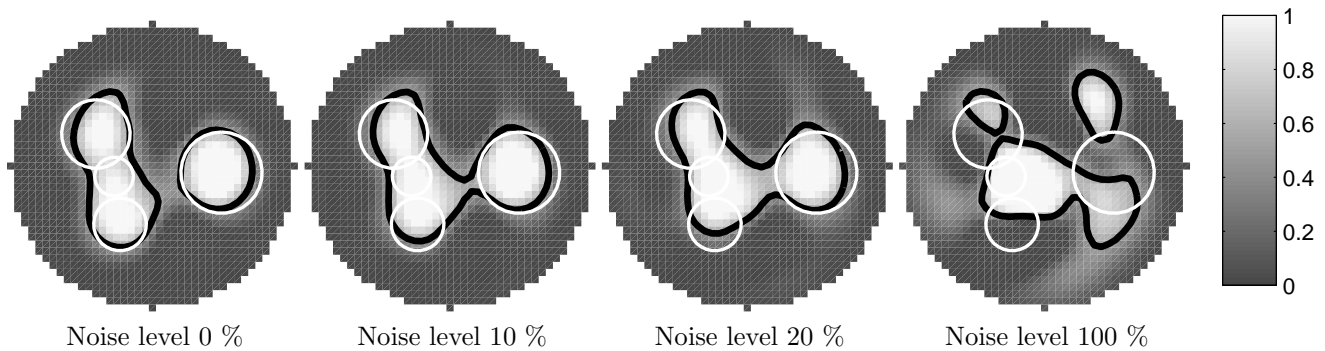


Figure 8: Example of the effect of additive Gaussian noise in inputs to reconstruction result. The gray scale shows the posterior probability of bubble in each pixel. The actual bubble is shown by the white circles and the segmented bubble by the black line.

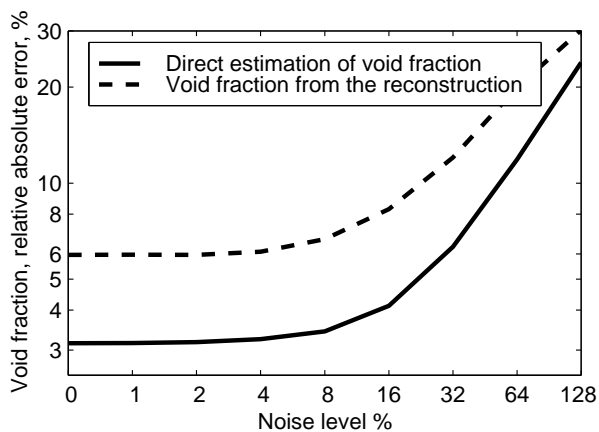


Figure 9: Effect of additive Gaussian noise to the direct estimation of the void fraction and estimation of void fraction from the reconstructed image.

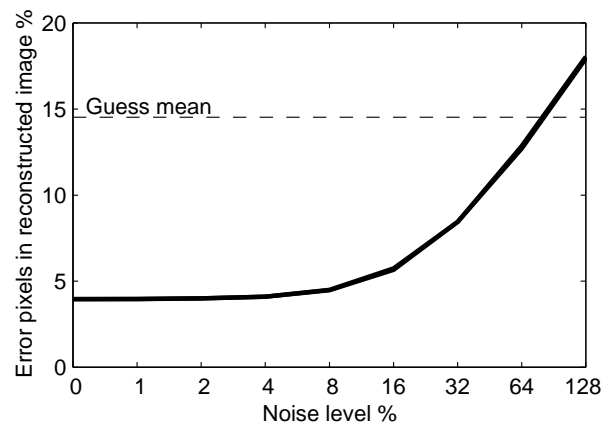


Figure 10: Effect of additive Gaussian noise to the reconstruction of the images. The dashed line corresponds to guessing the mean of training bubbles independent of the input potential.

## Acknowledgment

This study was partly funded by Technology Development Center TEKES Grant 40888/97 (Project PROMISE, *Applications of Probabilistic Modeling and Search*).

## References

- [1] M. Vauhkonen, J. Kaipio, E. Somersalo, and P. Karjalainen, "Electrical impedance tomography with basis constraints," *Inverse Problems* **13**(2), pp. 523–530, 1997.
- [2] A. Y. Nooralahiyan and B. S. Hoyle, "Three-component tomographic flow imaging using artificial neural network reconstruction," *Chemical Engineering Science* **52**(13), pp. 2139 – 2148, 1997. See also <http://www.elec-eng.leeds.ac.uk/staff/een6njb/Research/processtom.html>.
- [3] A. Adler and R. Guardo, "A neural network image reconstruction technique for electrical impedance tomography," *IEEE Transactions on Medical Imaging* **13**(4), pp. 594–600, 1994.
- [4] X. Ni, S. J. R. Simons, R. A. Williams, and X. Jia, "Use of PCA and neural network to extract information from tomographic images for process control," in *Proc. Frontiers in industrial process tomography*, vol. II, pp. 309–314, Engineering Foundation, (New York, USA), 1997.
- [5] C. M. Bishop, *Neural Networks for Pattern Recognition*, Oxford University Press, 1995.
- [6] R. M. Neal, *Bayesian Learning for Neural Networks*, vol. 118 of *Lecture Notes in Statistics*, Springer-Verlag, July 1996.
- [7] A. Vehtari and J. Lampinen, "Bayesian neural networks for image analysis," in *Proceedings of 11th Scandinavian Conference on Image Analysis SCIA '99*, (Kangerlussuaq, Greenland), June 1999.